Radiative Closure Studies for Clear Skies During the ARM 2003 Aerosol Intensive Observation Period

J. J. Michalsky[1], G. P. Anderson[2], J. Barnard[3], J. Delamere[4], C. Gueymard[5], S. Kato[6], P. Kiedron[7], A. McComiskey[8], and P. Ricchiazzi[9]

[1]Air Resources Laboratory, National Oceanic and Atmospheric Administration, Boulder, Colorado, joseph.michalsky@noaa.gov
[2]Air Force Research Laboratory/Battlespace Surveillance Innovation Center, USAF, Boulder, Colorado, gail.anderson@noaa.gov
[3]Pacific Northwest National Laboratory, Richland, Washington, james.barnard@pnl.gov
[4]Atmospheric and Environmental Research, Inc., Lexington, Massachusetts, jdelamer@aer.com
[5]Solar Consulting Services, Inc., New Smyrna Beach, Florida, chris@SolarConsultingServices.com
[6]Hampton University, Hampton, Virginia, s.kato@larc.nasa.gov
[7]Atmospheric Sciences Research Center, State University of New York, Albany, kiedron@asrc.cestm.albany.edu
[8]Cooperative Institute for Research in Environmental Sciences, University of Colorado, Boulder, allison.mccomiskey@noaa.gov
[9]Institute for Computational Earth System Science, University of California, Santa Barbara, paul@icess.ucsb.edu

Abstract

The Department of Energy's Atmospheric Radiation Measurement (ARM) program sponsored a large intensive observation period (IOP) to study aerosol during the month of May 2003 around the Southern Great Plains (SGP) Climate Research Facility (CRF) in north central Oklahoma. Redundant measurements of aerosol optical properties were made using different techniques at the surface as well as in vertical profile with sensors aboard two aircraft. One of the principal motivations for this experiment was to resolve the disagreement between models and measurements of diffuse horizontal broadband shortwave irradiance at the surface, especially for modest aerosol loading. This paper focuses on using the redundant aerosol and radiation measurements during this IOP to compare direct beam and diffuse horizontal broadband shortwave irradiance measurements and models at the surface for a wide range of aerosol cases that occurred during 30 clear-sky periods on 13 days of May 2003. Models and measurements are compared over a large range of solar-zenith angles. Six different models are used to assess the relative agreement among them and the measurements. Better agreement than previously achieved appears to be the result of better specification of input parameters and better measurements of irradiances than in prior studies. Biases between modeled and measured direct irradiances are less than 1%, and biases between modeled and measured diffuse irradiances are less than 2%.

1. Introduction

Achieving agreement between clear-sky shortwave irradiance models and measurements is a requirement for validating models, and it is the first step to further use of these models in more

complicated cloudy-sky analyses. However, recent efforts to achieve broadband shortwave radiative closure have met with some difficulties. Kato et al. (1997) looked at clear-sky data in the mid 1990s and found that direct beam irradiance (hereafter, direct irradiance) models and measurements agreed well. Halthore et al. (1997) reached a similar conclusion. Kato et al.'s (1997) diffuse horizontal broadband shortwave irradiance (hereafter, diffuse irradiance) measurements, however, were well below the modeled irradiance even though the uncertainties in the inputs and errors due to model assumptions were taken into account. Halthore et al. (1998) concluded, likewise, that models of diffuse irradiance were higher than measurements. This led to a reassessment of offsets in thermal pyranometers caused by the temperature gradient between the dome and thermopile of pyranometers that had been noted decades earlier (e.g., Gulbrandsen, 1978), but largely ignored. A series of papers resolved the offset issue by proposing methods to correct the error (Bush et al. 2000; Haeffelin et al. 2001; Dutton et al. 2001; and Michalsky et al. 2003). Halthore and Schwartz (2000) found that even with corrected offsets, diffuse irradiance measurements were persistently lower than models. Barnard and Powell (2002) confirmed the Halthore and Schwartz (2000) result for the SGP CRF, however, using data from the North Slope of Alaska ARM site near Barrow, they were able to achieve closure. In a recent paper using improved aerosol property inputs to the model, Halthore et al. (2004) were still unable to achieve closure at the SGP CRF in northern Oklahoma. In another recent paper where model input aerosol optical properties were carefully scrutinized, Henzing et al. (2004) were able to achieve closure between direct beam measurements and models, but found that models produced much higher diffuse irradiance for a mid-latitude site in the Netherlands.

This paper uses data from a major aerosol field experiment conducted between May 5, 2003, and May 30, 2003, at and above the central site of the SGP CRF, which is located midway between Lamont and Billings, Oklahoma, at 36.61° N and 97.49° W. One purpose of this aerosol intensive observation period (AIOP) was to obtain and compare redundant measurements of each aerosol optical property needed as model input to radiative transfer codes. The main purpose of this paper is to compute the direct and diffuse irradiance by six radiative transfer codes using these inputs that cover a wide range of aerosol optical thicknesses, solar zenith angles, and water vapor amounts, and to compare with the measured direct and the thermal-offset-corrected diffuse irradiance.

In section 2 the data used as input to the models and the radiation data used to compare to model calculations are described. The six models that are used to generate the results for the 30 cases are described in section 3. Results of the model-model and model-measurement comparisons are shown in section 4. The results and major conclusions are discussed in the final section.

2. Model Data Input and Radiation Measurements

Skies were screened for clear-sky periods using three sources of data. First, time series plots of broadband direct and diffuse data were used to assess the probability of clear skies. This was followed with plots of the multi-filter rotating shadow-band radiometer (MFRSR) 870-nm diffuse data (Harrison et al. 1994). This wavelength has little Rayleigh scattering, and even light cirrus noticeably affects the shape of the time series plots. A final step was to use the sky images from the YES, Inc. Total Sky Imager (TSI) to confirm the selection of clear-sky period identifications. Thirty cases were identified that included low to high sun angles and aerosol

loads that ranged over those typically observed for this site. Extremely low values of aerosol optical thickness (< 0.05) were not and are not generally observed in May.

The most important input variables in clear-sky solar radiation modeling of surface irradiance include aerosol information, specifically, column aerosol optical depth, single scattering albedo, and asymmetry parameter, all as a function of wavelength. The other key variables for clear-sky modeling are, in approximate order of importance, water vapor, ozone, and the spectral albedo of the surface that surrounds the sites where irradiance measurements are made.

Aerosol optical depth measurements were made with a normal incidence multi-filter radiometer (NIMFR), which is a modified MFRSR that looks directly at the sun with a 5.7º field of view. Optical depths are measured at five wavelengths including 415, 500, 615, 673, and 870 nm. Measurements are made every 20 seconds during all daylight hours. CIMEL sun-photometer measurements are also made at the ARM CRF as part of the AERONET network (Holben et al. 1998). For 13 of the 30 cases we compared CIMEL and NIMFR measurements at or near three wavelengths--500, 670, and 870 nm. Of the 39 comparisons three were not within the 95% uncertainty limits, as expected, and there was negligible bias between the measurement sets. In addition, Schmid et al. (2005) compared NIMFR measurements with the 14-channel Ames Airborne Tracking Sunphotometer (AATS-14) on 12 occasions when the instrument flew about 90 m above the ground-based NIMFR. They report root-mean squared differences and biases that were actually better that those between the AATS-14 and two CIMEL sun-photometers that operated during the campaign. For consistency we used the NIMFR aerosol optical depth in all calculations.

The single scattering albedos and asymmetry parameters used in the radiative transfer calculations were derived from ground-based in situ measurements made with the CRF's Aerosol Observing System (AOS). The AOS and derivation of the single scattering albedo is explained in Sheridan et al. (2001). The derivation of the asymmetry parameter is based on a method described in Wiscombe and Grams (1976). An improvement to the derivation of asymmetry parameter and its uncertainty is described in a paper based on data from this same IOP (Andrews et al. 2005). On occasion the AOS data were unavailable, and in those cases data from a backup system that was in the guest instrument facility (GIF) within 200 m of the CRF AOS were used. The two systems produced data that agreed to within their uncertainties when both were operating. The absorption data were measured at 550 nm using a Radiance Research model PSAP. The scattering data were measured at three wavelengths, including 450, 550, and 700 nm by two TSI, Inc. Model 3563 nephelometers operated in series with one held near 40% humidity and the other ramped between 40 and 90% humidity. All derived single scattering albedos and asymmetry parameters were adjusted to ambient humidity conditions using these data.

The water vapor column was obtained from the ARM data archive www.archive.arm.gov. These measurements are made every 20 seconds using a microwave radiometer, however, the five-minute-averaged data are used for this study. The derivation and uncertainty in column water vapor is explained in Liljegren (1994). Ozone data are obtained from the Total Ozone Mapping Spectrometer (TOMS) web site http://toms.gsfc.nasa.gov. For the two cases where TOMS data were not available Dobson data for Boulder, Colorado, obtained from the Climate Monitoring and Diagnostics Laboratory website www.cmdl.noaa.gov/ozwv/dobson were used. Even though

neither of these ozone columns is measured on site, the values obtained should add only insignificant uncertainty (< 0.2%) to the predicted broadband fluxes.

Spectral surface albedo input data were parameterized from the two downward looking multi-filter radiometer (MFR) heads that are on the 10-m tower over un-grazed pasture and at the 25-m level of the 60-m tower over a wheat field. MFR data were divided by up-looking MFRSR data to determine surface albedos at six wavelengths. Equal weighting of the surface albedos used in the calculations was based on the subjective observation that the site is surrounded mostly by wheat and pasture in equal proportions. The parameterization used for the surface albedo between 300 and 3000 nm is described in Michalsky et al. (2003). A straight line is fit between 300 and 700 nm using the four shortest wavelengths (415, 500, 615, and 673 nm) from the two MFRs. A constant value is determined using the average value of the two longest wavelengths (870 and 940 nm) from the two MFRs and used for all wavelengths between 750 and 1300 nm. A line connects the 700 and 750 nm points from each fit. Finally, a line connects the 1300 nm point and zero surface albedo at 3000 nm based on general tendencies for vegetation. Figure 1 illustrates how the wavelength-dependent surface albedo was determined for a single case. Since clear-sky surface albedos show solar-zenith angle and wavelength dependencies, the surface albedo is determined in this way for each observation.

The ground-based direct beam and diffuse horizontal shortwave irradiance data used in model comparisons was obtained from the CRF's radiation calibration facility (RCF) and GIF that are separated by no more than 200 m. An absolute cavity radiometer makes the preferred measurement of direct beam irradiance. Cavity measurements were made from the RCF for seven of the 30 cases studied. For the other direct beam measurements a pyrheliometer, Eppley model NIP, labeled A on the GIF observing stand was used. The diffuse horizontal irradiance data were obtained from two instruments on the GIF observing stand. The diffuse value used was an average of an Eppley 8-48 shaded pyranometer, which has no offset, and an offset-corrected Kipp & Zonen CM22. The offset correction applied in the latter case is a two-parameter fit as explained in Michalsky et al. (2005).

3. Models Used in the Downwelling Shortwave Calculations

The models used for the comparisons have low to moderate spectral resolution. The modeled direct beam and diffuse horizontal spectral irradiances are spectrally integrated to compare with broadband shortwave measurements. The extraterrestrial spectral irradiance assembled by Gueymard (2004) was used as the input spectrum unless stated otherwise in the model descriptions below. A surface albedo file that spanned the 300-3000 nm wavelength region was provided for each case. Table 1 contains information regarding the models and how inputs were applied for the 30 cases in this study.

Correlated-k distribution tables used in RAPRAD (Toon et al. 1989) were built based on the HITRAN 2000 database (Rothman et al. 1987) using a line-by-line code (LBLRTM, Clough et al. 1995). Absorption by water vapor, ozone, carbon dioxide and oxygen is included (Kato et al. 1999). To avoid assuming multiplication properties (Goody and Yung 1998) for overlapping bands, we fixed the minor gas concentration and built tables as a function of pressure, temperature and concentration of major gases. Because the multiplicative rule gives the

minimum transmission, the direct irradiance is larger by 0.4% compared to the direct irradiance using the multiplicative assumption.

RAPRAD was run with some modifications to the specified inputs. To extrapolate measured single scattering albedos and asymmetry parameters at 550 nm to other wavelengths, the single scattering albedo and asymmetry parameter are computed with Mie theory using the refractive index of sulfate (d'Almeida et al. 1991), a mode radius of 0.1, and assuming a lognormal distribution with a standard deviation of 1.4. These values are then scaled by the ratio of the computed to measured values at 550 nm.

MODTRAN™ 4.9, which calculates cloudy and clear sky irradiance, radiance, and transmittance, was used (Anderson et al. 2000). MODTRAN™'s historic 1 cm^{-1} band model is based on a two-parameter equivalent width band model (proportional to temperature and pressure) that employs large pre-stored spectral databases. With the addition of correlated-k (Lacis and Oinas, 1991), coupled with the automated flux output from the embedded DISORT (Stamnes et al. 1988) algorithm, the required inputs for this comparison are readily available. The band model parameters are derived directly from the spectral line data on HITRAN2K (Rothman et al. 2003), including all corrections and extensions before 2004. See http://cfa-www.harvard.edu/HITRAN/ for details. The code includes the CKD continua for water vapor, O_2, and N_2 (Clough et al. 1980; see http://rtweb.aer.com/), version CKD_2.4. Appropriate spectroscopic descriptions are available for each of 13 molecular species, plus cross sections for the heavy molecules (e.g., CFC's) in the HITRAN database. The band model approach is designed for temperature ranges between 180 and 320°K under conditions of local thermodynamic equilibrium only.

MODTRAN™ provides a selection of default options for inputs, but also allows the users to supply their own. Many of the user-supplied options were used in these calculations, including some newly written options (to be included in the next release of MODTRAN™ 4, version 9). The MODTRAN™ calculations for this study included those in Table 2 plus:

1. AOT (500nm) converted to AOT (550 nm)
2. Solar extraterrestrial irradiance: Gueymard (2004) was used; differences between the MODTRAN™ default vs. Gueymard are < 0.2%
3. Solar geometry: elevation angle, as in Table 2, converted to solar zenith angle

SMARTS is the Simple Model of the Atmospheric Radiative Transfer of Sunshine. It is a clear-sky code used to calculate the shortwave (280–4000 nm) direct beam and diffuse irradiance on any surface (Gueymard 1995, 2000). It is used extensively in solar energy research and applications. The code is very fast, easy to run and free. The latest beta version (2.9.4) is used here. At each wavelength, the individual atmospheric transmittances due to absorption by a maximum of 17 gas species (besides water vapor) are calculated from Lambert-Beer's law. An optical mass specific to each species is used for it, along with temperature-dependent absorption coefficients obtained by downgrading high-resolution spectroscopic cross-section data. For water vapor, parameterizations of the MODTRAN™ band model are used. To better simulate the radiometers' response, the optional circumsolar correction was turned on and a 5.7° angle was considered for both the pyrheliometer's field of view and the sky area blocked by the diffuse pyranometer's shading disk.

RRTM_SW calculates shortwave fluxes and heating rates in 14 contiguous bands (Mlawer et al. 1998; Clough et al. 2004) using the correlated-k method of radiative transfer and the discrete ordinates radiative transfer program DISORT (Stamnes et al. 1988). The k-distributions were obtained from absorption coefficients obtained from the well-validated, line-by-line radiative transfer model LBLRTM, thus providing a traceable link from RRTM_SW to observations done at the highest spectral resolution. RRTM_SW is suitable for use as a reference to improve the performance of GCM shortwave codes. Modeled sources of extinction include water vapor, carbon dioxide, ozone, methane, oxygen, Rayleigh scattering, and aerosols. For this comparison, the aerosol optical depths are derived from the Angstrom relationship, with spectrally constant single-scattering albedos and asymmetry parameters. The solar source function used is based on theoretical radiative transfer calculations for the solar atmosphere (Kurucz 1992).

Santa Barbara DISORT Atmospheric Radiative Transfer (SBDART, version 2.4) is a widely-used code for calculations of radiative transfer in both cloudy and clear atmospheres (Ricchiazzi et al. 1998; www.crseo.ucsb.edu/esrg/pauls_dir). It is based on the DISORT multiple scattering radiative transfer module, and includes models for the important scattering and absorption processes that affect solar and infrared transmission. The code is quite flexible and provides options to run with three models of extraterrestrial source spectra, six standard atmospheric models (McClatchey et al. 1972), and a variety of optical models for clouds and aerosols. To satisfy differing requirements of speed and accuracy, SBDART can be run in either the standard low-resolution mode that uses gas absorption band models from LOWTRAN, or in a more accurate correlated-k mode. When running in the high-accuracy mode, SBDART uses correlated-k optical depths generated from line-by-line transmission calculations. This capability was originally developed in a program named SBMOD (Yang et al, 2000), which is the name used to identify the high resolution SBDART runs in this study.

For SBDART and SBMOD the aerosol optical depth was interpolated between measured aerosol optical depth wavelengths. For wavelengths beyond the measured short and long wavelength endpoints an extrapolation in optical depth using an Angstrom coefficient (α) of 1 was assumed.

4. Comparison Results

Thirty clear-sky cases were selected from 13 days during the IOP. Table 2 contains most of the input parameters used to model the direct and diffuse horizontal irradiances detected at the surface. This table indicates the range of circumstances that were modeled. Times ranged from early morning to late afternoon, including times near solar noon, consequently, solar elevations were as low as 12º and as high as 75º. Aerosol loads ranged from 0.05 to 0.49 at 500 nm with some changes in the wavelength dependence of the aerosol extinction. A common way to express the aerosol optical depth wavelength behavior is as the slope of a linear least squares fit to a plot of the natural log of the aerosol optical depth versus the natural log of the wavelength in micrometers. That slope is commonly designated α, which is listed in Table 2 for all 30 cases. For comparison a typical value of α for continental aerosols is 1.3. Integrated column water vapor varied between 1.0 and 3.6 cm. Ozone had a modest variation during the selected days with extreme values of 291 and 350 Dobson units. Of particular note is the fact that single scattering albedos (column labeled *ssa*) were unexceptional with all mid-visible values between

0.88 and 0.97, and most were in the middle of this range. The aerosol asymmetry parameters (column labeled *g*) ranged between 0.51 and 0.69.

Table 3 contains the measured direct beam irradiance (the seven cavity values are embolden in Tables 3 and 5) and the calculated results from the six models for all 30 cases. The next to last line of Table 3 (in bold type) is the average direct irradiance for all 30 cases. The bottom line lists the average percent difference for all thirty cases. The six, modeled direct irradiances are from 0.5% low to 0.9% high; this range is smaller than the estimated uncertainty in the direct irradiance measurements without even considering the model uncertainties. Table 4 contains the diffuse irradiance measurements and the model results for all 30 cases. Again, the mean measured and modeled irradiances are listed on the next to last line and the average percent difference for all 30 cases is on the bottom of Table 4. The range in measurement/model diffuse irradiance difference is between -1.3% and +1.8%. This is a remarkable improvement over earlier results and is smaller than the diffuse measurement uncertainty.

Gueymard (2003) contains a sensitivity study for direct beam only. He found that the primary contributions to uncertainty arise from aerosol optical depth and water vapor column. Table 5 contains SBMOD model results and IOP measurements with one simple change in the model inputs. The model was run with an aerosol optical depth of 0.01 subtracted from every wavelength. Using this lower aerosol optical depth, the comparison of measurements and the SBMOD model results is significantly worse with higher direct beam and lower diffuse irradiance. An uncertainty of 0.01 in aerosol optical depth is a typical uncertainty for well-made aerosol optical depth measurements. Of course, all inputs and radiation measurements contain uncertainty and a paper by McComiskey et al. (2005) is in preparation to illustrate how uncertainties in model inputs and measurements propagate and affect both direct normal and diffuse horizontal irradiance comparisons.

5. Discussion and Conclusions

The results are very encouraging in that the measurements fall in the middle of the range of all six models' results for both the direct and diffuse irradiance. The direct measurements have model results that are both higher and lower. The diffuse measurements are within the bounds of the model results, with very small differences compared to the latest published, clear-sky model and measured diffuse irradiance comparisons (Halthore and Schwartz 2000; Halthore et al. 2004; Henzing et al. 2004). While the previous papers have emphasized that the clear-sky comparisons are problematic on low aerosol optical depth days, there is no apparent correlation between model and measurements differences and the level of aerosol loading. The relatively low-aerosol optical depth days of May 5th, 11th, and 12th do not show a significantly greater difference with regard to discrepancies than do the other days.

The SMARTS model differs in one respect from the others in that it attempts to mimic the way measurements are made. Direct beam measurements include some of the solar aureole because pyrheliometers have an aperture that is either 5º or 5.7º, depending on the particular instrument, compared to the 0.5º disk subtended by the sun; diffuse measurements exclude approximately the same sized aureole. For the conditions of May 10th (large AOD and large zenith angle), this circumsolar correction was a maximum and added about 10 W/m^2 (or 3.6%) to the calculated

direct normal irradiance and removed about 3 W/m^2 (or 2.2%) from the calculated diffuse horizontal irradiance.

The sensitivity of the comparisons to model input and irradiance measurement uncertainties will be discussed in greater detail in another paper (McComiskey et al. 2005), but the improvement in model and measurement agreement by invoking a rather small change in optical depth as presented in the previous section illustrates the high sensitivity of these comparisons to the aerosol optical depth input. In analyzing the early comparisons among the models for this paper, it was discovered that a large difference was caused by the manner in which the models handled the aerosol optical depth wavelength dependence. Most of the models simply used an optical depth that followed the Angstrom expression

$$\tau = \beta\lambda^{-\alpha}$$

using the values of optical depth at 500 nm and alpha in Table 2 to calculate aerosol optical depth at all other wavelengths. SBDART and SBMOD interpolate aerosol optical depth between the five NIMFR wavelengths and assume that the aerosol optical depth at 415 applies to all shorter wavelengths and the aerosol optical depth at 870 applies at all longer wavelengths. Changing this algorithm to assume a λ^{-1} aerosol optical depth dependence outside the measured aerosol wavelength range using the 415 and 870 end points as anchors produced about a 10 W/m^2 increase in modeled direct irradiance and about a 4 W/m^2 decrease in modeled diffuse irradiance yielding significant improvements in the agreement with measured values.

In general, the extinction of real aerosols cannot be described using fixed aerosol models from the literature. Therefore, the SMARTS model uses its built-in simplified treatment based on the AOD at 500 nm and a two-tier Angstrom law, with distinct average values of the wavelength exponent (α) for the 280–500 and 500–4000 nm wavebands. This was specifically done here by linearly fitting the measured aerosol optical depth values from the five available NIMFR channels (415–870 nm) to the log-transformed Angstrom's equation, separately for these two wavebands. The broadband-averaged alpha value indicated in Table 2 was, therefore, not used. Note, however, that the two band-average values of α obtained were generally found close to each other for all days except May 5th, when the 280–500 nm value was negative at about –0.3, considerably less than the 500–4000 nm value of about +0.4; this indicates the influx of a somewhat atypical mix of aerosols on that day.

Referring to Table 1, the surface albedos were treated differently in the six models. Files of surface albedo were supplied for the 300-3000 nm range. Most models simply used the values at 300 nm and 3000 nm for wavelengths shorter and longer than these wavelengths, respectively. Some models set the values outside the given range to zero. For clear skies these assumptions will make no difference in direct beam results and little difference in diffuse irradiance given the small contribution of infrared radiation in clear skies and the small contribution of ultraviolet radiation below 300 nm. Surface albedos at the six fixed wavelengths, which were used to parameterize the surface albedo for the full range of wavelengths in the input files, were also made available for the model runs. One model was run using those measured values directly, linearly interpolating between the measurements and using the endpoint albedos for wavelengths outside the range of the measurements. This resulted in less than a 0.1% change in diffuse

irradiance. Most significantly, if the surface albedo is derived from the measured broadband surface albedo and that constant value is used for all wavelengths, the calculated diffuse irradiance increases on average by 7%.

Since ground-based values of single scattering albedo and asymmetry parameter were used, it can be argued that the column values of these parameters may not be well represented in these calculations. Andrews et al. (2004) found that the ground-based measurements at the AOS are, on average, fairly representative of the column. If anything, the column-averaged single scattering albedo tends to be slightly lower than the surface value for an average profile. A lower single scattering albedo would slightly reduce the diffuse model results. The asymmetry parameter tends to be greater in the layers just above the surface and then smaller at even higher altitudes, thus it is less clear whether the column-averaged asymmetry parameter would produce any difference in modeled diffuse irradiance at the surface (E. Andrews, private communication). During the IOP, elevated layers of aerosol above the site were detected. In the last days of the month these aerosol layers originated from Siberian forest fires. Ferrare et al. (2005) report single scattering albedos of 0.96-0.98 for these elevated aerosol layers on the 25th and 27th of May. These values are slightly, but not significantly greater than the surface-based AOS single scattering albedos, therefore, they should not significantly affect the calculated diffuse irradiance.

The modeled and measured differences for the direct beam and diffuse horizontal irradiances in terms of root-mean-square (rms) differences and biases are summarized in Figure 2. The hatched boxes are rms differences for direct normal and diffuse irradiances. The solid boxes represent the biases in terms of modeled – measured irradiances. Rms differences for direct normal irradiance range between 0.9 and 1.2%; biases range between –0.7 and 0.8%. Rms differences for diffuse irradiances range between 3.6 and 4.5%; biases range between –1.1 and 1.9%. Results for both direct and diffuse fall within the combined uncertainties of the models and measurements.

Only one model used a significantly different wavelength range to define the shortwave. SBMOD's longwave cut-off was 2950 nm, while the other models included radiation out to 3800 nm or beyond. Based on a MODTRAN™ sensitivity run, a cutoff at 3000 nm should result in direct being underestimated, relative to a longwave cut-off of 4000 nm, by 5-6 W/m^2 on average and produce less than a 0.5 W/m^2 underestimate in diffuse. Therefore, if the shortwave cutoff were extended to 4000 nm we would expect the SBMOD direct model and measurement difference to all but disappear, and the diffuse overestimate would improve slightly. Only one model RRTM_SW did not use the Gueymard (2004) extraterrestrial spectrum; it used the Kurucz (1992) theoretical spectrum that integrates to 1368 W/m^2, which is 2 W/m^2 larger than Gueymard (2004). Using the latter spectrum one would expect the RRTM_SW bias to increase by about 1 W/m^2.

In summary, broadband solar models and measurements seem to have merged as a result of better specification of input parameters and better measurements of irradiances than in prior studies. However, improving the uncertainties of the inputs and irradiance measurements is an unfinished task. Further effort is warranted in testing more cases for very low aerosol optical depth days that tend to occur in mid to late Autumn at the SGP CRF. Finally, these models should be tested spectrally against a carefully calibrated shortwave spectral irradiance data set in

order to ensure that the cancellation of errors in different portions of the spectrum is not responsible for the excellent agreement achieved in this study.

Acknowledgments

We thank Mary Jane Bartholomew for providing the CIMEL aerosol optical depths for comparison to the NIMFR data. Alexander Berk provided assistance with regard to setting up the MODTRAN™ calculations. John Augustine carefully edited the final version. The National Oceanic and Atmospheric Administration's Climate Program supported this work as did the Office of Science (BER), U. S. Department of Energy, through Interagency Agreement No. DE-AI02-04ER63703. The Aerosol IOP was made possible through the financial support of the U. S. Department of Energy's Atmospheric Radiation Measurement program.

References

Anderson, G. P., et al. (2000), MODTRAN4: Radiative transfer modeling for remote sensing in algorithms for multispectral, hyperspectral, and ultraspectral imagery VI, Proceedings of SPIE 4049-16, pp. 176-183, Orlando, Florida, 24 April.

Andrews, E., P. J. Sheridan, J. A. Ogren, and R. Ferrare (2004), In situ aerosol profiles over the Southern Great Plains cloud and radiation test bed site: 1. Aerosol optical properties, *J. Geophys. Res.*, 109, D06208, doi:10.1029/2003JD004025.

Andrews, E., et al. (2005), Comparison of methods for deriving aerosol asymmetry parameter, submitted to *J. Geophys. Res.*

Barnard J. C., and D. M. Powell (2002), A comparison between modeled and measured clear-sky radiative shortwave fluxes in Arctic environments, with special emphasis on diffuse radiation, *J. Geophys. Res.*, 107 (D19), 4383, doi:10.1029/2001JD001442.

Bush, B. C., F. P. J. Valero, A. S. Simpson, and L. Bignone (2000), Characterization of thermal effects in pyranometers: A data correction algorithm for improved measurement of surface insolation, *J. Atmos. Ocean. Tech.*, 17, 165-175.

Clough, S. A. and M. J. Iacono (1995), Line-by-line calculation of atmospheric fluxes and cooling rates, 2, Application to carbon dioxide, ozone, methane, nitrous oxide and the halocarbons, *J. Geophys. Res.*, 100, 16519-16535.

Clough, S.A., F.X. Kneizys, R. Davis, R. Gamache and R. Tipping (1980), Theoretical line shape for H2O vapor: Application to the continuum, in *Atmospheric Water Vapor*, edited by A. Deepak, T.D. Wilkerson and L.H. Ruhnke, p. 52, Academic Press, New York.

Clough, S.A., M.W. Shephard, E.J. Mlawer, J.S. Delamere, M.J. Iacono, K. Cady-Pereira, S. Boukabara, P.D. Brown (2004), Atmospheric radiative transfer modeling: a summary of the AER codes, *J. Quant. Spectros. Radiat. Transfer*, 91, 233-244.

d'Almeida, G. A., P. Koepke, and E. P. Shettle (1991), *Atmospheric Aerosols: Global Climatology and Radiative Characteristics*, 561 pp., A. Deepak Publishing, Hampton, Virginia.

Dutton, E. G., J. J. Michalsky, T. Stoffel, B. W. Forgan, J. Hickey, D. W. Nelson, T. L. Alberta, and I. Reda (2001), Measurement of broadband diffuse solar irradiance using current commercial instrumentation with a correction for thermal offset errors, *J. Atmos. Ocean. Tech.*, 18, 297-314.

Ferrare, R. et al. (2005), Evaluation of Daytime Measurements of Aerosols and Water Vapor made by an Operational Raman Lidar over the Southern Great Plains, submitted to *J. Geophys. Res.*

Goody, R. M. and Y. L. Yung (1989), *Atmospheric Radiation*, 2nd ed., p. 127, Oxford University Press, New York.

Gueymard, C. (1995), SMARTS2, Simple Model of the Atmospheric Radiative Transfer of Sunshine: Algorithms and performance assessment, *Rep. FSEC-PF-270-95,* Florida Solar Energy Center, Cocoa Beach, Florida.

Gueymard, C. (2001), Parameterized transmittance model for direct beam and circumsolar spectral irradiance, *Solar Energy*, 71, 325-346.

Gueymard, C. A. (2003), Direct solar transmittance and irradiance predictions with broadband models. Part II: validation with high-quality measurements, *Solar Energy*, 74, 381-395. Corrigendum (2004), 76, 515.

Gueymard, C. A., (2004), The sun's total and spectral irradiance for solar energy applications and solar radiation models, *Solar Energy*, 76, 423-453.

Gulbrandsen, A. (1978), On the use of pyranometers in the study of spectral solar radiation and atmospheric aerosols, *J. Appl. Meteorol.*, 17, 899-904.

Haeffelin, M., S. Kato, A. M. Smith, C. K. Rutledge, T. P. Charlock, and J. R. Mahan (2001), Determination of the thermal offset of the Eppley precision spectral pyranometer, *Appl. Opt.*, 40, 472-484.

Halthore, R. N., S. E. Schwartz, J. J. Michalsky, G. P. Anderson, R. A. Ferrare, B. N. Holben, H. M. Ten Brink (1997), Comparison of model estimated and measured direct-normal solar irradiance, *J. Geophys. Res.*, 102, 29991-30002.

Halthore, R. N., S. Nemesure, S. E. Schwartz, D. G. Emre, A. Berk, E. G. Dutton, and M. H. Bergin (1998), Models overestimate diffuse clear-sky irradiance: A case for excess atmospheric absorption, *Geophys. Res. Lett.*, 25, 3591-3594.

Halthore, R. N. and S. E. Schwartz (2000), Comparison of model-estimated and measured diffuse downward irradiance at surface in cloud-free skies, *J. Geophys. Res.*, 105, 20165-20177.

Halthore, R. N., M. A. Miller, J. A. Ogren, P. J. Sheridan, D. W. Slater, and T. Stoffel (2004), Further developments in closure experiments for diffuse irradiance under cloud-free skies at a continental site, *Geophys. Res. Lett.*, 31, L07111, doi:10.1029/2003GL019102.

Halthore, R.N., et al. (2004) Intercomparison of shortwave radiative transfer codes and measurements, Submitted to *J. of Geophys. Res.*

Harrison, L., J. Michalsky, and J. Berndt (1994), Automated multifilter rotating shadow-band radiometer: An instrument for optical depth and radiation measurements, *Appl. Opt.*, 33, 5118-5125.

Henzing, J. S., W. H. Knap, P. Stammes, A. Apituley, J. B. Bergwerff, D. P. J. Swart, G. P. A. Kos, and H. M. ten Brink (2004), Effect of aerosols on the downward shortwave irradiances at the surface: Measurements versus calculations with MODTRAN4.1, *J. Geophys. Res.*, 109, D14204, doi:10.1029/2003JD004142.

Holben, B. N., et al. (1998), AERONET--A federated instrument network and data archive for aerosol characterization, *Remote Sens. Environ.*, 66, 1-16.

Kato, S., T. P. Ackerman, E. E. Clothiaux, J. H. Mather, G. G. Mace, M. L. Wesely, F. Murcray, and J. Michalsky (1997), Uncertainties in modeled and measured clear-sky surface shortwave irradiances*, J. Geophys. Res.*, 102, 25,881-25,898.

Kato, S., T. P. Ackerman, J. H. Mather, and E. E. Clothiaux (1999), The k-distribution method and correlated-k approximation for a shortwave radiative transfer model, *J. Quant. Spectros. Radiat. Transfer*, 62, 109-121.

Kurucz, T. L. (1992), Synthetic infrared spectra, *Infrared Solar Physics, I.A.U. Symposium 154*, D. M. Rabin and J. T. Jeffries (eds.), Kluwer Academics, Norwell, Massachuetts.

Lacis, A. A. and V. Oinas (1991), A description of the correlated-k distribution method for modeling non-gray gaseous absorption, thermal emission, and multiple scattering in vertically inhomogeneous atmospheres, *J. Geophys. Res.*, 96, 9027-9063.

Liljegren, J. C. (1994), Two-channel microwave radiometer for observations of total column precipitable water vapor and cloud liquid water path, in *Fifth Symposium on Global Climate Change Studies*, pp. 262-269, American Meteorological Society, 25-28 January, Nashville, Tennessee.

Liljegren, J. C., S. A. Boukabara, K. Cady-Pereira, and S. A. Clough (2005), The effect of the half-width of the 22-ghz water vapor line on the retrievals of temperature and water vapor profiles with a twelve-channel microware radiometer, *IEEE Transactions on Geosciences and Remote Sensing*, 43, xxxx-xxxx.

McClatchey, R. A., R. W. Fenn, J. E. A. Selby, F. E. Volz, and J.S. Garing (1972), *Optical Properties of the Atmosphere*, 3rd ed., Air Force Cambridge Research Laboratories, L.G. Hanscom Field, Bedford, Massachuetts.

McComiskey, A., S. E. Schwartz, P. Ricchiazzi, J. A. Ogren, J. J. Michalsky, E. Lewis (2005), Direct aerosol forcing: Calculation from observables and sensitivites to inputs, in *Proceedings of The Fifteenth ARM Science Team Meeting*, 14-18 March, Daytona Beach, Florida.

Michalsky, J.J., et al. (2003), Results from the first ARM diffuse horizontal shortwave irradiance comparison, *J. Geophys. Res.*, 108(D3), 4108, doi:10.1029/2002JD002825.

Michalsky, J., Q. Min, J. Barnard, R. Marchand, and P. Pilewskie (2003), Simultaneous spectral albedo measurements near the Atmospheric Radiation Measurement Southern Great Plains (ARM SGP) central facility, *J. Geophys. Res.*, 108(D8), 4254, doi:10.1029/2002JD002906.

Michalsky, J. J. et al. (2005), Toward the development of a diffuse horizontal shortwave irradiance working standard, *J. Geophys. Res.*, 110, D06107, doi:10.1029/2004JD005265.

Mlawer, E.J. and S.A. Clough (1998), Shortwave clear-sky model-measurement intercomparison using RRTM, in *Proceedings of the Eighth ARM Science Team Meeting*, 23-27 March, Tucson, Arizona.

Ricchiazzi, Paul, Yang, Shiren, Gautier, Catherine, Sowle, David (1998), SBDART: A Research and Teaching Software Tool for Plane-Parallel Radiative Transfer in the Earth's Atmosphere, *Bulletin of the American Meteorological Society,* 79, 2101-2114.

Rothman, L.S., et al. (1987), The HITRAN database: 1986 edition, *Appl. Opt.*, 26, 4058-4097.

Rothman , L. S., et al. (2003), The HITRAN molecular spectroscopic database: edition of 2000 including updates through 2001, *J. Quant. Spectros. Radiat. Transfer*, 82, 5–44.

Schmid, B., et al. (2005), How well can we measure the vertical profile of tropospheric aerosol extinction?, *J. Geophys. Res.* (submitted).

Sheridan, P. J., D. J. Delene, and J. A. Ogren (2001), Four years of continuous surface aerosol measurements from the Department of Energy's Atmospheric Radiation Measurement Program Southern Great Plains Cloud and Radiation Testbed site, *J. Geophys. Res.*, 106, 20735-20747.

Stamnes, K., S. C. Tsay, W. J. Wiscombe, and K. Jayaweera (1988), Numerically stable algorithm for discrete-ordinate-method raditive transfer in multiple scattering and emitting layered media, *Appl. Opt*., 27, 2502-2509.

Toon, O. B., C. P. Mckay, and T. P. Ackerman (1989), Rapid calculation of radiative heating rates and photodissociation rates in inhomogeneous multiple scattering atmosphere, *J. Geophys. Res.*, 94, 16287-16301.

Wiscombe, W.J. and G.W. Grams (1976), The backscattered fraction in two-stream approximations, *J. Atmos. Sci.*, 33.

Yang, S. R., Ricchiazzi, P., and Gautier, C. (2000), Modified correlated k-distribution methods for remote sensing applications, *J. Quant. Spectros. Radiat. Transfer*, 64 (N6):585-608.

Model	λ range	λ resolution	Surface Albedo	Radiative Transfer	Web Site	References
RAPRAD	240-4600 nm	32 discrete bands	300-3000 nm, as specified, with fixed 300 nm and 3000 nm values above and below these λs.	Correlated-k and Delta-2 stream		Toon et al. (1989) Kato et al. (1999)
MODTRAN 4.9	280-4000 nm	5 cm^{-1}	Same as above.	Correlated-k and DISORT, 8-stream	www.vs.afrl.af.mil/Division/VSBYB/modtran4.html	Anderson et al. (2000)
SMARTS 2.9.4	280-4000 nm	0.5 nm, if < 400 nm 1 nm, 400-1705 nm 5 nm, if > 1705 nm	Same as above.	Modified 2-stream	rredc.nrel.gov/solar/models/SMARTS/	Gueymard (1995) Gueymard (2000)
RRTM_SW, ver. 2.5	263-3846 nm	14 discrete bands	Used albedos at 415, 500, 615, 673, 870, and 940 nm and scaled with tabulated vegetative albedos.	Correlated-k and DISORT, 8-stream	rtweb.aer.com	Mlawer et al. (1998) Clough et al. (2004)
SBDART 2.4	250-4500 nm	Variable with higher resolution at shorter wavelengths	300-3000 nm, as specified, with zero values below 300 and above 3000 nm.	DISORT, 4-stream	www.crseo.ucsb.edu/esrg/pauls_dir	Ricchiazzi et al. (1998)
SBMOD 1.0	280-2950 nm	5 nm	300-3000 nm, as specified, with zero values below 300 and above 3000 nm.	Correlated-k and DISORT, 8-stream	www.crseo.ucsb.edu/esrg/pauls_dir	Yang et al. (2000)

Table 1. Model feature descriptions.

Date	CST	sun elev. (°)	AOT 500 nm	α	ssa	g	H_2O(cm)	O_3 (DU)
5-May-03	645	13.3	0.053	0.22	0.89	0.58	1.31	336
	800	28.2	0.055	0.21	0.93	0.69	1.38	336
	910	42.1	0.053	0.20	0.93	0.56	1.44	336
	1200	68.8	0.074(0.063)*	0.29	0.92	0.54	1.51	336
	1600	38.9	0.073	0.25	0.95	0.55	1.82	336
	1800	15.0	0.082	0.36	0.93	0.59	1.98	336
6-May-03	1730	21.1	0.140	1.30	0.93	0.57	1.77	350
	1815	12.2	0.137	1.32	0.92	0.55	1.76	350
7-May-03	730	22.5	0.138	1.34	0.93	0.63	2.03	337
	930	46.4	0.098	1.22	0.85	0.54	2.04	337
9-May-03	930	46.7	0.257(0.265)*	0.63	0.95	0.64	1.01	318
	1130	67.1	0.296(0.304)*	0.66	0.94	0.61	1.17	318
	1230	70.8	0.266(0.266)*	0.64	0.94	0.61	1.47	318
10-May-03	700	17.0	0.489(0.526)*	0.93	0.95	0.66	1.62	301
11-May-03	700	17.2	0.076	1.05	0.97	0.51	1.07	312
	920	45.1	0.083	1.06	0.97	0.57	1.12	312
	1230	71.3	0.085(0.055)*	0.96	0.94	0.58	1.18	312
	1500	51.5	0.071(0.057)*	0.88	0.96	0.55	1.17	312
12-May-03	730	23.3	0.081	1.18	0.88	0.57	1.58	323
	950	51.1	0.083(0.080)*	1.18	0.93	0.56	1.59	323
20-May-03	1400	63.7	0.198(0.203)*	1.40	0.93	0.64	2.33	bldr-294
22-May-03	800	30.4	0.195	1.40	0.94	0.66	2.51	bldr-309
27-May-03	1300	73.1	0.295(0.284)*	1.38	0.94	0.60	1.39	334
	1600	41.7	0.301	1.35	0.95	0.61	1.47	334
28-May-03	730	24.9	0.231	1.61	0.93	0.61	3.08	320
	1800	17.9	0.199	1.57	0.95	0.62	2.79	320
29-May-03	830	36.9	0.144	1.28	0.94	0.61	2.89	291
	1230	75.0	0.127(0.123)*	1.16	0.95	0.60	2.92	291
30-May-03	1130	70.6	0.168(0.166)*	1.20	0.92	0.58	3.59	293
	1445	56.8	0.158(0.157)*	1.36	0.94	0.61	3.26	293

*AERONET values in ()

Table 2. The key model inputs except for surface albedos.

direct(W/m^2) (measured)	sbdart direct	raprad direct	smarts direct	sbmod direct	modtran direct	rrtm direct
604	607	608	601	605	598	597
827	818	821	814	815	822	811
913	906	911	904	902	915	901
968	956	962	959	952	962	952
859	858	859	856	855	862	852
571	578	575	567	574	566	567
643	647	659	651	645	648	652
474	473	482	481	472	469	482
669	664	679	668	662	669	669
882	878	889	880	874	889	880
757	760	765	764	757	766	757
798	803	808	808	799	816	800
816	823	829	827	819	832	819
263	273	276	281	278	270	274
681	677	690	680	675	682	682
910	906	915	910	902	921	909
971	964	972	969	960	985	966
936	934	942	938	931	953	936
750	742	754	744	740	752	747
909	914	924	918	911	926	917
854	853	865	859	850	865	858
694	689	701	694	686	698	694
844	833	842	844	830	847	838
732	717	729	729	715	729	724
601	595	610	603	594	606	604
534	524	538	533	523	529	534
774	772	780	775	769	783	774
903	900	906	904	897	914	901
865	858	875	863	855	876	859
844	844	852	848	841	857	844
761.5	**758.8** (0.3% lo)	**767.3** 0.9% hi	**762.4** 0.3% hi	**756.3** (0.5% lo)	**766.9** 0.7% hi	**760.0** (0.01% lo)

Table 3. Direct beam measurements and six model results.

diffuse(W/m^2) (measured)	sbdart diffuse	raprad diffuse	smarts diffuse	sbmod diffuse	modtran diffuse	rrtm diffuse
51	48	50	49	47	49	49
70	73	73	74	72	72	75
78	79	79	79	78	81	81
95	98	98	98	97	104	101
90	87	88	87	87	92	90
64	59	61	60	59	60	60
83	79	79	78	78	81	78
58	55	58	55	54	56	54
82	82	82	82	81	83	80
96	89	88	88	88	92	88
184	183	180	183	182	184	186
220	215	212	216	214	217	217
205	203	201	204	202	207	206
128	124	128	127	126	124	124
60	60	60	60	59	61	59
87	93	91	91	92	94	92
91	103	101	101	102	104	102
84	90	89	89	89	92	90
67	67	67	67	66	68	65
95	91	89	89	90	94	90
148	145	143	143	144	147	142
114	112	111	109	112	114	110
185	189	186	185	188	196	186
160	164	161	159	163	168	161
106	102	102	102	101	104	100
81	81	81	80	80	82	79
105	103	101	101	102	107	102
117	119	117	115	117	123	117
134	133	129	131	132	137	131
121	124	121	121	123	127	122
108.6	**108.3** (0.4% lo)	**107.5** (0.7% lo)	**107.4** (1.1% lo)	**107.5** (1.3% lo)	**110.7** 1.8% hi	**107.9** (0.08% lo)

Table 4. Diffuse horizontal measurements and six model results.

direct(W/m^2) (measured)	sbmod(-0.01) direct	diffuse(W/m^2) (measured)	sbmod(-0.01) diffuse
604	629	51	44
827	831	70	66
913	915	78	72
968	962	95	91
859	868	90	81
571	594	64	56
643	661	83	75
474	492	58	52
669	677	82	77
882	886	96	83
757	766	184	177
798	807	220	208
816	827	205	196
263	286	128	125
681	695	60	55
910	914	87	86
971	969	91	94
936	942	84	82
750	757	67	62
909	922	95	84
854	859	148	138
694	698	114	107
844	838	185	182
732	724	160	158
601	607	106	98
534	538	81	77
774	781	105	97
903	905	117	111
865	864	134	126
844	850	121	117
761.5	**768.8**	**108.6**	**102.6**
	1.3% hi		(6.2% lo)

Table 5. SBMOD model results with 0.01 subtracted from the optical depth at each wavelength.

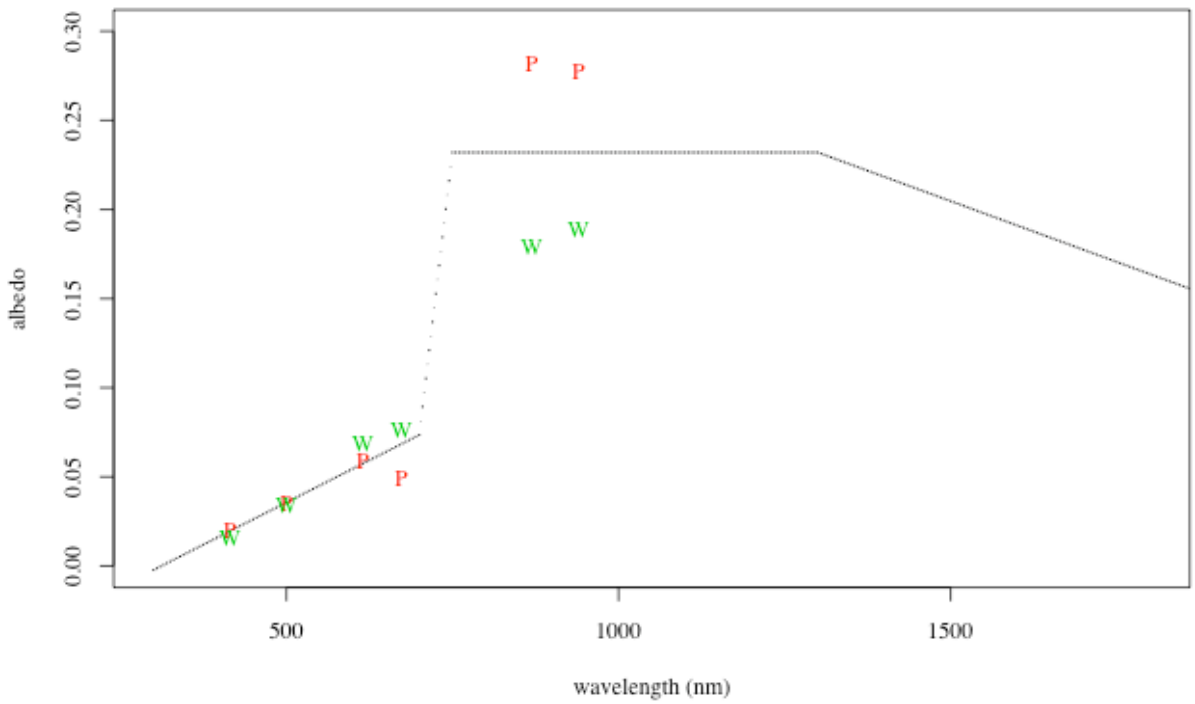

Figure 1. Parameterized surface albedo input (dotted black line). The individual measurements of wheat (W) and pasture (P) surface albedos are also shown.

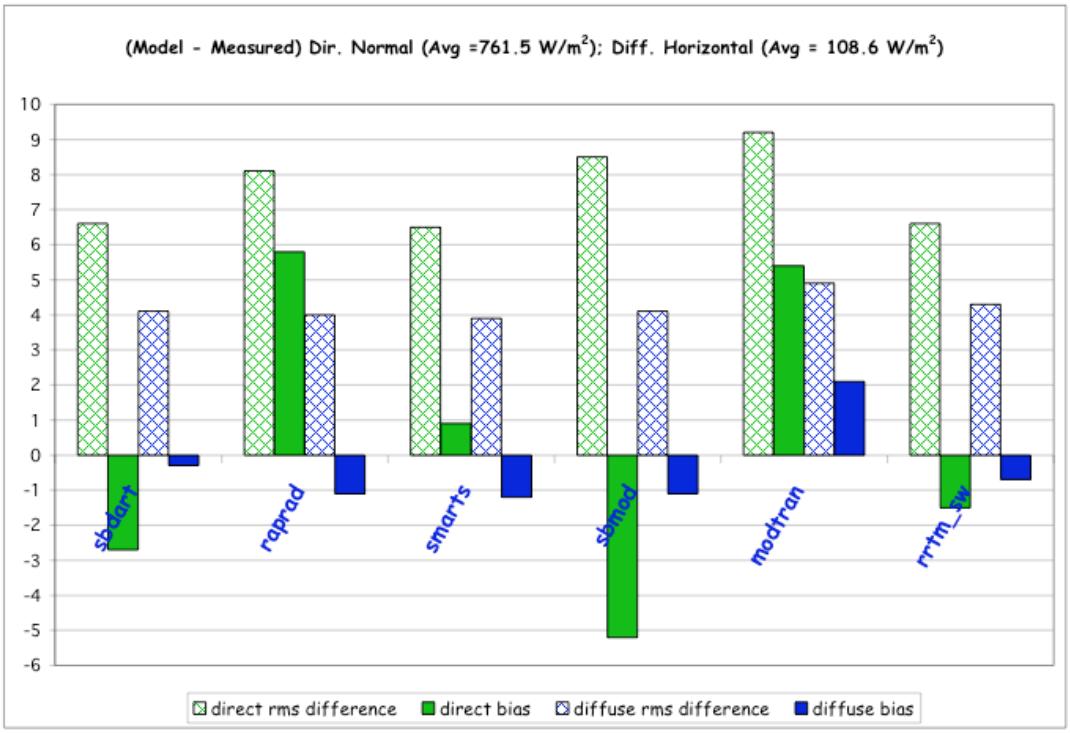

Figure 2. Thirty-cases of modeled - measured results in W/m^2 for direct beam and diffuse horizontal irradiances.